DOI: 10.1002/ange.201408483

$LiNbO_3$-type Magnetic Oxynitride

$MnTaO_2N$: Polar $LiNbO_3$-type Oxynitride with a Helical Spin Order**

*Cédric Tassel, Yoshinori Kuno, Yoshihiro Goto, Takafumi Yamamoto, Craig M. Brown, James Hester, Koji Fujita, Masanobu Higashi, Ryu Abe, Katsuhisa Tanaka, Yoji Kobayashi, and Hiroshi Kageyama**

Abstract: *The synthesis, structure, and magnetic properties of a polar and magnetic oxynitride $MnTaO_2N$ are reported. High-pressure synthesis at 6 GPa and 1400 °C allows for the stabilization of a high-density structure containing middle-to-late transition metals. Synchrotron X-ray and neutron diffraction studies revealed that $MnTaO_2N$ adopts the $LiNbO_3$-type structure, with a random distribution of O^{2-} and N^{3-} anions. $MnTaO_2N$ with an "orbital-inactive" Mn^{2+} ion (d^5; $S=5/2$) exhibits a nontrivial helical spin order at 25 K with a propagation vector of [0,0,δ] ($\delta \approx 0.3$), which is different from the conventional G-type order observed in other orbital-inactive perovskite oxides and $LiNbO_3$-type oxides. This result suggests the presence of strong frustration because of the heavily tilted MnO_4N_2 octahedral network combined with the mixed O^{2-}/N^{3-} species that results in a distribution of (super)-super-exchange interactions.*

Oxynitrides show properties that cannot be attained by simple oxides or simple nitrides.[1] Experimentally, transition-metal oxynitrides with the perovskite structure have been extensively explored, with a variety of functions discovered such as water splitting photocatalysis in $BaTaO_2N$,[2] non-toxic colorful pigments in $Ca_{1-x}La_xTaO_{2-x}N_{1+x}$ ($0 \le x \le 1$),[3] colossal magnetoresistivity in $EuNbO_2N$ and $EuWO_2N$,[4] and high permittivity in $SrTaO_2N$.[5] These properties originate from the differences between N^{3-} and O^{2-} in valence, ionic radius,[6] electronegativity, and polarizability.[7]

However, most of the transition-metal oxynitrides synthesized so far consist of early transition metals such as Ti, Zr, Nb, Ta, V, Mo, and W in the d^0 (and rarely d^1) state.[1b,8] This is primarily a result of the synthesis process of oxynitrides, where the corresponding solid oxide precursors are reacted with ammonia at elevated temperatures (thermal ammonolysis). The highly reducing atmosphere during thermal ammonolysis does not permit middle-to-late transition metals to form oxynitrides without being reduced to elemental metals or metal nitrides. For this reason, only a handful of magnetic oxynitrides are known including $PrVO_{2.24}N_{0.76}$, $LaVO_{2.09}N_{0.91}$,[9] $NdVO_2N$,[10] $SrMoO_2N$,[11] $SrWO_2N$,[12] $Li_{7.9}MnN_{5-x}O_x$ ($x \approx 1.7$),[13] and $Mn_2(MnTa_3)N_{6-x}O_{2+x}$ ($0 \le x \le 1$).[14] However, they do not exhibit any long-range magnetic ordering (apart from that originating from *A*-site rare-earth elements). To the best of our knowledge, only $Sr_2FeMoO_{6-x}N_x$ ($x = 0.3$ and 1) is reported to exhibit long-range magnetic ordering.[15]

The high-pressure synthesis is known to provide access to high-density crystalline phases. It also allows rational preparation of new mixed anion compounds with a designed chemical composition using appropriate starting materials. A growing number of oxyfluorides, oxychlorides, and other mixed anion compounds have been developed using this approach.[16] For example, we successfully obtained a stoichiometric perovskite oxyhydride $SrCrO_2H$ using SrO, SrH_2 and Cr_2O_3 as starting reagents.[17] Few nonmagnetic oxynitrides have been prepared including perovskites $RE ZrO_2N$ (RE = Pr, Nd, Sm) (1200–1500 °C at 2 GPa to 3 GPa)[18] and a spinel Ga_3O_3N (1500–1700 °C at 5 GPa).[19] Here, we report on the high pressure synthesis of a novel magnetic oxynitride $MnTaO_2N$ with $3d^5$ Mn^{2+} ($S = 5/2$) and $5d^0$ Ta^{5+}. It crystallizes in a non-centrosymmetric $LiNbO_3$-type (LN-type) structure. Historically, high pressure has been actively applied to stabilize LN-type oxides ABO_3 (A = Fe, Mn, Zn, Mg and B = Ti, Sn) with small divalent *A*-site cations.[20] $Mn^{2+}Ti^{4+}O_3$ is of the ilmenite-type at ambient pressure, while the application of pressure induces a transformation to the LN-type structure.[21] Thus, the synthesis of LN-type $MnTaO_2N$ can be

[*] Dr. C. Tassel, Y. Kuno, Y. Goto, Dr. T. Yamamoto, Dr. K. Fujita, Dr. M. Higashi, Prof. R. Abe, Prof. K. Tanaka, Dr. Y. Kobayashi, Prof. H. Kageyama
Graduate School of Engineering, Kyoto University
Kyoto 615-8510 (Japan)
E-mail: kage@scl.kyoto-u.ac.jp
Dr. C. Tassel
The Hakubi Center for Advanced Research, Kyoto University
Kyoto 606-8501 (Japan)
Dr. C. M. Brown
Center for Neutron Research
National Institute of Standards and Technology
Gaithersburg, MD 20899 (USA)
and
Department of Chemical Engineering, University of Delaware
Newark, DE 19716 (USA)
Dr. J. Hester
Bragg Institute
Australian Nuclear Science and Technology Organization
Locked Bag 2001, Kirrawee DC NSW 2232 (Australia)
Prof. R. Abe, Prof. H. Kageyama
CREST (Japan)

[**] This work was supported by the Hakubi Project funding, Grant-in-Aid for Scientific Research A (No. 24248016) and the Young Scientist Grant B (No. 25810040) from MEXT, and CREST project. We thank Mr. Takuya Aoyama and Prof. T. Kimura at Osaka University for valuable discussions and Mr. K. Nakano and Mr. T. Kuge for assistance, respectively, in neutron diffraction and second harmonic generation experiments.

Supporting information for this article is available on the WWW under http://dx.doi.org/10.1002/anie.201408483.

rationalized in terms of a charge compensated substitution of "Ta^{5+}/Ti^{4+} and N^{3-}/O^{2-}" from LN-type $MnTiO_3$. Remarkably, $MnTaO_2N$ undergoes magnetic long-range order at 25 K, a rare example of magnetic order in transition-metal oxynitrides. Furthermore, we found a nontrivial helical spin order, as opposed to the isostructural and isoelectronic LN-type $MnTiO_3$ with a conventional *G*-type structure (T_N = 28 K), with a small spin canting caused by Dzyaloshinskii–Moriya (DM) interactions.[22]

The high-pressure synthesis of $MnTaO_2N$ was conducted using a cubic multianvil press. TaON and MnO were intimately mixed in stoichiometric ratio in a nitrogen filled glovebox ($O_2 < 0.1$ ppm and $H_2O < 0.1$ ppm), loaded in a Pt cell and heated for one hour at various temperatures up to 1400 °C and at pressures up to 6 GPa. As shown in Figure 1, $MnTaO_2N$ was yielded when reacted at 1400 °C and 6 GPa.

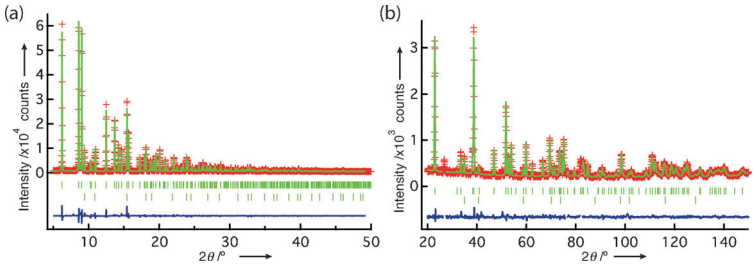

Figure 1. Structural characterizations of $MnTaO_2N$ by Rietveld refinement of a) SPXRD and b) NPD (BT-1, NCNR) collected at 295 K. Red crosses, green solid line, and blue solid line represent observed, calculated, and difference intensities, respectively. The upper and lower green ticks indicate the positions of the Bragg peaks of $MnTaO_2N$ and a minority cubic impurity phase (about 2 wt%), respectively.

The synchrotron powder X-ray diffraction (SPXRD) pattern of the product was indexed with a rhombohedral unit cell, $a = 5.34039(3)$ Å and $c = 14.0799(1)$ Å. The inspection of the Bragg peaks showed extinction conditions compatible with the *R*3*c* (No. 161) and $R\bar{3}c$ (No. 167) space groups. We note that both SPXRD and neutron powder diffraction (NPD) patterns contain small impurity peaks belonging to an unknown phase with a cubic face-centered structure, as well as residual TaON. To determine the presence or absence of the inversion center of the main product, we conducted second harmonic generation (SHG) experiments because the SHG properties are related to a third-rank polar tensor. SHG response at room temperature was clearly observed, from which we conclude that the target compound is acentric. Rietveld refinement was hence performed using the LN-type structure with Ta placed at site 6*a* (0,0,0) and Mn at 6*a* (0,0,*z*) (where *z* is about 0.28). Oxygen and nitrogen atoms were assumed to be disordered at the 18*b* (*x*,*y*,*z*) site since there is no indication of anion order in SPXRD. A simultaneous refinement was performed on the SPXRD/NPD data with a constraint on the O/N occupancy such that the sum resulted in a fully occupied site. While there is little scattering contrast between O and N for X-rays, NPD can provide reliable information on the anion composition because of the large difference in scattering lengths of oxygen and nitrogen (N = 9.36 fm and O = 5.81 fm). The dual refinement converged readily to reliable factors $R_{wp} = 7.73\,\%$, GOF = 2.72 for SPXRD and $R_{wp} = 7.25\,\%$, GOF = 1.31 for NPD (Figure 1 and Table 1; GOF = goodness of fit). Refining the occupancy of Mn, Ta, and O/N from unity did not improve the result. The final anion composition refined to $MnTaO_{1.96(6)}N_{1.04}$. Complementary experiments by combustion elemental analysis and energy dispersive X-ray spectrometry (EDS), respectively, gave 4.4(3) wt% N, in reasonable agreement with the theoretical value of 4.97 wt%, and a Mn/Ta ratio of 1. Local distortions by different anions (N^{3-}/O^{2-}) might be present, but the high symmetry of our material hampered the observation of such effect and would be better probed using other techniques, such as total scattering.

Table 1: Structural parameters of $MnTaO_2N$ from simultaneous Rietveld refinement of SPXRD and NPD at 295 K.[a] Error bars indicate one standard deviation in the final digit.

Atom	Site	*g*	*x*	*y*	*Z*	U_{iso} (100 Å^2)
Mn^{2+}	6*a*	1	0	0	0.28093(2)	0.54(3)
Ta^{5+}	6*a*	1	0	0	0	0.77(1)
O^{2-}	18*b*	0.654(19)	0.0527(6)	0.3455(6)	0.0733(1)	0.39(11)
N^{3-}	18*b*	0.346	0.0527	0.3455	0.0733(1)	0.39(11)

[a] Space group *R*3*c* (No. 161), $a = 5.34039(3)$ Å, $c = 14.0799(1)$ Å. $R_{wp} = 7.73\,\%$, $R_p = 5.30\,\%$, GOF = 2.72 for SPXRD and $R_{wp} = 7.25\,\%$, $R_p = 5.73\,\%$, GOF = 1.31 for NPD.

A polyhedral representation of the crystal structure of $MnTaO_2N$ is given in Figure 2a. The MnO_4N_2 octahedron is face-shared with the TaO_4N_2 octahedron, which results in the formation of three short (2.12 Å) and three long (2.39 Å) Mn-O(N) bonds (Figure 2b). These values are close to those observed in other LN-type manganese oxides.[20c,22] The TaO_4N_2 octahedron is distorted as well with three short (1.99 Å) and three long (2.11 Å) Ta-O(N) bonds, which are comparable with those of perovskite oxynitrides $ATaO_2N$ (*A* = alkali earth).[23]

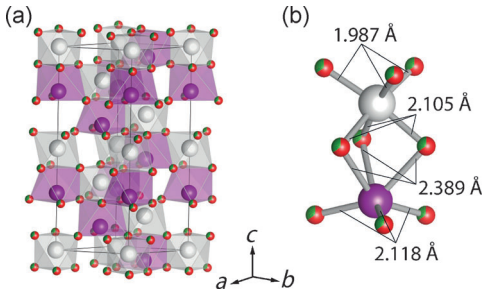

Figure 2. a) Crystal structure of $LiNbO_3$-type $MnTaO_2N$. b) Face-shared MnO_4N_2-TaO_4N_2 octahedral dimer. Purple, gray, red, and green spheres represent Mn, Ta, O, and N, respectively. The O and N atoms are randomly distributed at the anionic site.

A measure of octahedral distortion, Δ, was calculated according to the equation given in Ref. [24]. We obtained Δ =

36.2×10^{-4} for the MnO_4N_2 octahedron, which is slightly larger than 15.1×10^{-4} and 26.9×10^{-4} for MnO_6 in LN-type $MnTiO_3$ and $MnSnO_3$, respectively. The larger distortion of Mn octahedron is potentially arising from a larger cationic charge (repulsion) across the shared octahedral face. We also found that $\Delta=8.3\times10^{-4}$ for TaO_4N_2 is smaller than 38×10^{-4} for TiO_6 in $MnTiO_3$, but larger than 2.8×10^{-4} for SnO_6 in $MnSnO_3$, which may be related to a weaker second-order Jahn–Teller (SOJT) effect or the random O^{2-}/N^{3-} environment. Using the atomic displacement from the centrosymmetric structure, the spontaneous polarization along the hexagonal c axis is calculated to be about 51.5 $\mu C\,cm^{-2}$, when the nominal ionic charges of the constituent ions are assumed. This value is comparable with 68.6 $\mu C\,cm^{-2}$ and 55.1 $\mu C\,cm^{-2}$ in $MnTiO_3$ and $MnSnO_3$, respectively.[20c]

Shown in Figure 3 is the magnetic susceptibility of the insulating $MnTaO_2N$ measured in an applied field of 0.1 T. At high temperatures, the experimental data follows a Curie–Weiss law. A fit of the inverse susceptibility data in the temperature range $200\,K\le T\le300\,K$ gives an effective magnetic moment μ_{eff} of 6.03(8) μ_B/Mn, in agreement with the expected value for a high spin Mn^{2+} ion ($S=5/2$), $\mu_{eff}=5.91\,\mu_B$. A significantly large Weiss temperature of $\theta=-233(6)$ K indicates the presence of strong antiferromagnetic (AFM) spin-spin interactions. Despite the strong AFM correlation, however, the linear dependence of the reciprocal susceptibility is seen at lower temperatures. The susceptibility exhibits a sharp cusp at 25.5 K, implying the occurrence of AFM order.

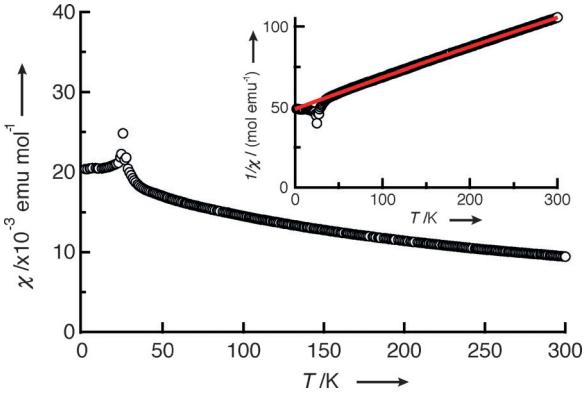

Figure 3. Temperature dependence of the magnetic susceptibility of $MnTaO_2N$ measured at 0.1 T. The inset shows the inverse susceptibility, where the red line represents the Curie–Weiss fit.

To gain direct evidence for long-range AFM order, NPD patterns at low temperatures were collected at BT-1 in NIST and at Wombat in ANSTO. As shown in Figure 4 (and in Figure S1 in the Supporting Information), we found several non-nuclear peaks at 6 K, together with the nuclear reflections observed at higher temperatures. With increasing temperature, these additional peaks begin to reduce in intensity with a slight and gradual shift of position, before finally vanishing above 30 K. Together with the susceptibility result, this observation strongly suggests the magnetic origin of these reflections. The magnetic propagation vector at each temperature below T_N was determined using five magnetic peaks and the K-Search program included in the FULLPROF suite.[25] It is found that the magnetic structure is defined by the propagation vector along the hexagonal c axis, $k=[0,0,\delta]$ (where δ is about 0.3).

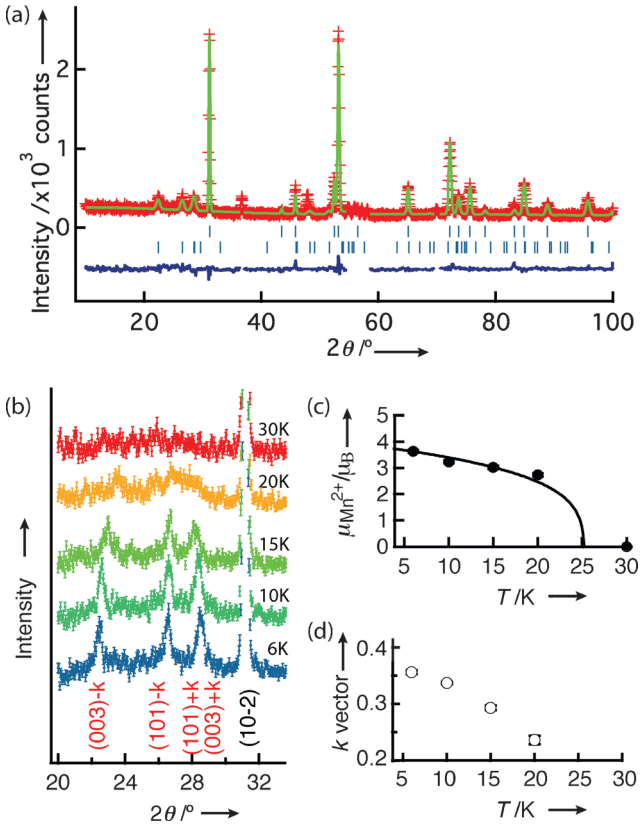

Figure 4. a) Rietveld refinement of NPD for $MnTaO_2N$ at 6 K (BT-1, $\lambda=2.0775$ Å). Red crosses, green solid line, and blue solid line stand for the observed, calculated, and difference intensities, respectively. Upper and lower ticks indicate the positions of the crystal and magnetic Bragg reflections. Peaks around $2\theta=36.4$–37°, 54.5–58.5°, 47.15–48.55°, originated from TaON are eliminated from the refinement. b) Temperature dependence of the magnetic peaks for $T\le30$ K. c) Temperature dependence of the magnetic moment of Mn^{2+} and d) the k-vector $[0,0,\delta]$ as determined by the structural refinement. The solid lines are a guide to the eye.

Possible magnetic structures were derived from a magnetic representation analysis using BasIreps.[25] Three irreducible representations were determined using the $R3c$ space group and the obtained k-vector at 6 K, [0,0,0.36]. Among them, refinements using the first two models with spins aligned parallel or antiparallel to the c axis failed to reproduce the experimental peaks. The representation of the last one is composed of four vectors that dictate ferromagnetic (FM) and AFM structures within the ab plane. Data fitting using a combination of these vectors provided the best result with $R_{wp}=8.25\,\%$ and GOF = 1.48 (see Figure 4a). As shown in Figure 5c and d, the Mn^{2+} moments lie in the ab plane, the in-plane moments are parallel to each other, and the FM layers are stacked along the hexagonal c axis with a rotation of $\approx158.6°$ at 6 K. The refined k-vector (i.e., δ in $[0,0,\delta]$) slightly decreases with increasing temperature (Figure 4d). The

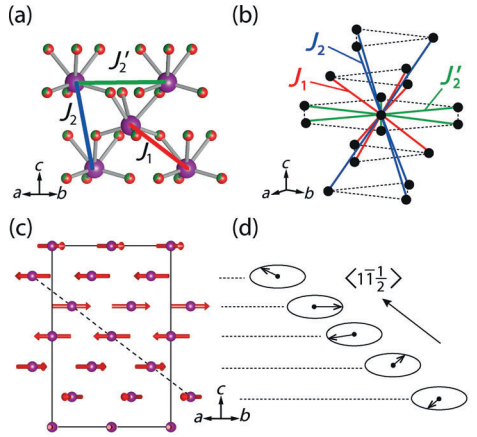

Figure 5. a) A corner-shared MnO_6 octahedral network with the NN (J_1) and NNN (J_2 and J_2') exchange paths. b) Magnetic interactions between Mn atoms: NN J_1 (red, 3.869 Å×6), the out-of-plane NNN J_2 (blue, 5.612 Å×6) and the in-plane NNN J_2' (green, 5.327 Å×6). c) Helical spin structure of $MnTaO_2N$ with a propagation vector of [0,0,0.356] at 6 K. The magnetic moments lay within the hexagonal *ab* plane. d) The spin rotation along $\langle 1\ -1\ 1/2\rangle$, which is equivalent to the pseudo-cubic [100].

helical rotation angle increases only slightly to 166.5° ($\delta = 0.22$) at 20 K. The temperature dependence of the refined magnetic moment is plotted in Figure 4c. The magnetic moment at 6 K is 3.63 μ_B, which is lower than the expected value of 5.0 μ_B for Mn^{2+} in a high spin state. We note, however, that this value is similar to that of $MnTiO_3$ (3.9 μ_B)[22] and strongly suggests the existence of strong frustration as pointed out from the magnetic susceptibility measurements.

It is well-known that structural, chemical and physical properties of ABO_3 perovskite oxides can be understood systematically from the Goldschmidt tolerance factor *t*. The ideal cubic perovskite is stable when $t \approx 1$. For $t < 1$, various types of BO_6 octahedral tilting occur.[26] For example, an anti-phase rotation along the cubic [111] direction leads to rhombohedral structures denoted as $a^-a^-a^-$ in the Glazer notation.[27] Under high pressure, compounds with a more extensive tilting ($t < 0.75$) are stabilized, leading to a transformation to other structural types including the LN-type structure.[26a] Here, it should be stressed that this transformation is topotactic, with the BO_6 network preserved in the LN-type structure. Since the LN-type structure has interpenetrated corner-shared octahedral networks of AO_6 and BO_6 (see Figure 5a), each network in the LN-type structure, AO_6 or BO_6, can be compared with the BO_6 network in perovskite.

This fact enables one to interpret magnetic properties of $MnTaO_2N$ with the corner-shared MnX_6 network (X = O, N), in comparison with the MO_6 octahedral network in insulating perovskite oxides AMO_3 (M = magnetic ion) that has been extensively studied and established. In AMO_3, the magnetism is dominated by the AFM nearest neighbor (NN) coupling, J_1, through (nearly linear) *M*-O-*M* superexchange pathways. On the basis of the Goodenough–Kanamori rule, J_1 is suppressed when the octahedral tilting increases (or *t* decreases) and the *M*-O-*M* angle deviates from the ideal 180°. Importantly, this distortion enhances the AFM next nearest neighbor (NNN) interactions, J_2, via super-superexchange *M*-O-O-*M* pathways and introduces magnetic frustration into the system.

In $MnTaO_2N$, we found a large difference between T_N (25 K) and $|\theta|$ (233 K). In addition to this difference, the observed helical order implies a fairly strong competition of magnetic interactions, which is reasonable, given the small *t* value of 0.77 in this compound. Using the above knowledge on perovskite, it can be argued that the strong frustration in $MnTaO_2N$ arises from competing NN (J_1) and NNN (J_2) interactions. The heavily tilted MnO_4N_2 octahedra (ω = 22.54° along the pseudo-cubic [111], which is much larger than those for perovskites ($0° \le \omega < 20°$)[26a]) result in the Mn-*X*-Mn angle of 121.8°.

Figure 5a and 5b shows that six NN J_1 bonds are equivalent and are antiferromagnetic due to the 121.8° bridging angle. On the other hand, there are two types of NNN couplings: one is the out-of-plane interaction J_2 (×6) and the other is the in-plane interaction J_2' (×6). Although the determination of the sign and the magnitude of super-superexchange coupling J_2 and J_2' (via several Mn-*X*-*X*-Mn pathways) is not straightforward, we can deduce from the in-plane FM spin order below T_N that J_2' is either ferromagnetic, or antiferromagnetic but is much weaker in magnitude than J_1. On the other hand, the helical rotation along the *c* axis indicates that frustration arises from out-of-plane interactions. Therefore, J_2 should be antiferromagnetic and comparable in magnitude with J_1.

We would like to point out that insulating perovskites mostly experience the *non-frustrated* *G*-type spin structure with all neighboring spins aligned anti-parallel to each other. This is not surprising given the predominance of J_1 (over J_2, J_3, J_4,…).[28] Different types of spin structures like *A*-type and *CE*-type are sometimes seen, but they appear only when complex factors such as itineracy, orbital/charge degrees of freedom, and magnetic interactions with the *A*-site rare earth ions are at play. Some examples are $LaMn^{3+}O_3$ (*A*-type),[29] $La_{0.5}Ca_{0.5}Mn^{3.5+}O_3$ (*CE*-type),[29] and $SrFe^{4+}O_3$,[30] $DyMn^{3+}O_3$,[31] $TbMn^{3+}O_3$ (helical order).[32] In this regard, the helical spin order in $MnTaO_2N$ with orbital-inactive Mn^{2+} ions (d^5; $S = 5/2$) is remarkable. The frustration index $|\theta|/T_N$ of 9.2 in $MnTaO_2N$ is fairly large compared with those of conventional orbital-inactive perovskite oxides (d^3, d^5) such as $BiCrO_3$ ($|\theta|/T_N = 2.75$,[33] $t = 0.85$), $LuCrO_3$ ($|\theta|/T_N = 3.35$, $t = 0.85$)[34] and $LuFeO_3$ ($|\theta|/T_N = 1.92$, $t = 0.84$).[28c] It is interesting to see that all the known LN-type oxides ($MnTiO_3$, $MnSnO_3$, $PbNiO_3$, $FeTiO_3$) also adopt the *non-frustrated* *G*-type structure, apart from a small canting caused by DM interactions.[35] Note that the frustration factors of these LN-type oxides are smaller: $|\theta|/T_N = 6$, 2.5, 2.4 and 2.2 for $MnTiO_3$, $MnSnO_3$,[20c] $PbNiO_3$,[36] and $FeTiO_3$,[20d] respectively. Interestingly, a metallic perovskite $Mn^2V^{4+}O_3$ with V 3d band electrons exhibits an incommensurate spin structure by the *A*-site (Mn^{2+}) ions via RKKY interaction.[37]

A complete understanding of the magnetism will require further experimental as well as theoretical investigations in the future. Yet it is highly possible that the mixed anion nature of $MnTaO_2N$ plays a crucial role in directing the helical structure. In $MnTaO_2N$, there exist Mn-N-Mn and Mn-O-Mn bonds which bring two inequivalent J_1 couplings, while Mn-O-

O-Mn, Mn-O-N-Mn, Mn-N-N-Mn bonding yield (at least) three inequivalent J_2 (and J_2') couplings. The mixed anionic environment may also affect the anisotropic exchange, dipolar interactions and crystal field anisotropy.[38] These mixed-anion effects would effectively enhance frustration and gives the nontrivial spin ordering in $MnTaO_2N$. It has been recently shown that oxynitrides favor *cis* coordinated octahedra owing to more covalent bonding with N-2p orbitals (vs. O-2p).[23c] Future investigations using pair distribution function analysis techniques as was performed in perovskite $BaTaO_2N$[39] could highlight the effect of such local constraints on the magnetic properties.

In conclusion, we have demonstrated that the high-pressure approach allows the preparation of a manganese oxynitride $MnTaO_2N$ with the polar LN-type structure. Notably, this material exhibits a helical spin order at 25 K with the propagation vector of $[0,0,\delta]$ (δ is about 0.3). This spin structure possibly arises from strong frustration between NN and NNN interactions and is different from the (canted) *G*-type order observed in isostructural, isoelectronic oxide counterparts. This material offers an advanced opportunity for developing magnetic polar materials. The synthesis of the solid solution $Mn(Ta_{1-x}Ti_x)O_2(N_{1-x}O_x)$ will be thus an interesting future challenge since the end members have different spin structures so that a phase transition is naturally expected. Since the discovery of multiferroic behavior in $TbMnO_3$,[40] compounds with helical magnetic structures have been extensively studied including $Ni_3V_2O_8$,[41] $MnWO_4$,[42] $CuFeO_2$[43] and CuO.[44] Despite the lack of a weak FM component in the present material, LN-type structure is polar in nature so that if weak FM is introduced by, for example, chemical substitution, it may become a new multiferroic material. It would be also exciting if one is able to synthesize other magnetic LN-type oxynitrides such as $MTaO_2N$ ($M = Fe^{2+}$, Ni^{2+}, Cu^{2+}, Co^{2+}). Finally, the high-pressure synthesis serves as an efficient tool to generate a number of magnetic oxynitrides of other structural types, which cannot be obtained by conventional ammonolysis reactions at high temperatures.

Experimental Section

TaON was synthesized, as previously reported,[45] using Ta_2O_5 (99.99%, Rare Metallic) heated at 850°C for 15 h under a NH_3 flow (5 N, Air Liquide, 20 mL min^{-1}). The stoichiometric mixture of MnO (99.9%, Rare Metallic) and TaON were used as starting reagents for the synthesis of $MnTaO_2N$. The synthesis of $MnTaO_2N$ was attempted under pressures in the 2–7 GPa range and at temperatures between 1000°C and 1400°C. Mixed powders were first pressed using a cubic anvil press to a target pressure and after heating to a target temperature in 15 minutes, the temperature was stabilized for one hour, then quenched to room temperature within 3 min, followed by a slow release of the pressure. SPXRD experiments were performed on a Debye–Scherrer camera at the BL02B2 beamline at SPring-8 ($\lambda = 0.42023$ Å). The NPD data for refinement were collected between 25 K and 385 K using a Cu(311) or Ge(311) monochromator ($\lambda = 1.5401$ Å and $\lambda = 2.0775$ Å, respectively) on BT-1 at NIST Center for Neutron Research (NCNR) and the Wombat diffractometer using a Ge115 monochromator ($\lambda = 2.71877$ Å) at ANSTO. Structural refinements were carried out using JANA2006[46] and FULLPROF.[25] EDS was collected by an Oxford x-act detector mounted on a Hitachi S-3400N scanning electron microscope. The magnetic data was obtained using a superconducting quantum interference device (SQUID) MPMS-XL (Quantum Design) in the temperature range of 2 K and 300 K. Optical second harmonic generation was tested for ungraded powders at RT using a pulsed Nd:YAG laser ($\lambda = 1064$ nm, pulse duration: 25 ps, repetition rate: 10 Hz) as the light source. Certain commercial equipment, instruments, or materials are identified in this document. Such identification does not imply recommendation or endorsement by the National Institute of Standards and Technology nor does it imply that the products identified are necessarily the best available for the purpose.

Received: September 24, 2014
Published online: November 21, 2014

Keywords: helical spin order · high-pressure chemistry · transition metals · magnetic oxynitrides · mixed anion phases

[1] a) A. Fuertes, *Dalton Trans.* **2010**, *39*, 5942; b) A. Fuertes, *J. Mater. Chem.* **2012**, *22*, 3293.
[2] a) M. Higashi, R. Abe, T. Takata, K. Domen, *Chem. Mater.* **2009**, *21*, 1543; b) K. Maeda, D. Lu, K. Domen, *Angew. Chem. Int. Ed.* **2013**, *52*, 6488; *Angew. Chem.* **2013**, *125*, 6616.
[3] M. Jansen, H. P. Letschert, *Nature* **2000**, *404*, 980.
[4] a) M. Yang, J. Oró-Solé, A. Kusmartseva, A. Fuertes, J. P. Attfield, *J. Am. Chem. Soc.* **2010**, *132*, 4822; b) A. B. Jorge, J. Oró-Solé, A. M. Bea, N. Mufti, T. T. M. Palstra, J. A. Rodgers, J. P. Attfield, A. Fuertes, *J. Am. Chem. Soc.* **2008**, *130*, 12572.
[5] Y.-I. Kim, P. M. Woodward, K. Z. Baba-Kishi, C. W. Tai, *Chem. Mater.* **2004**, *16*, 1267.
[6] R. Shannon, *Acta Crystallogr. Sect. A* **1976**, *32*, 751.
[7] L. Pauling, *The Nature of the Chemical Bond*, 3rd ed., Cornell University Press, Ithaca, NY, **1960**.
[8] a) S. G. Ebbinghaus, H.-P. Abicht, R. Dronskowski, T. Müller, A. Reller, A. Weidenkaff, *Prog. Solid State Chem.* **2009**, *37*, 173; b) P. Bacher, P. Antoine, R. Marchand, P. L'Haridon, Y. Laurent, G. Roult, *J. Solid State Chem.* **1988**, *77*, 67; c) R. Marchand, F. Pors, Y. Laurent, *Ann. Chim. Sci. Mater.* **1991**, *16*, 553; d) G. Liu, X. Zhao, H. A. Eick, *J. Alloys Compd.* **1992**, *187*, 145; e) P. Antoine, R. Assabaa, P. L'Haridon, R. Marchand, Y. Laurent, C. Michel, B. Raveau, *Mater. Sci. Eng. B* **1989**, *5*, 43; f) F. Pors, R. Marchand, Y. Laurent, P. Bacher, G. Roult, *Mater. Res. Bull.* **1988**, *23*, 1447; g) N. Kumar, A. Sundaresan, C. N. R. Rao, *Mater. Res. Bull.* **2011**, *46*, 2021.
[9] J. Oró-Solé, L. Clark, N. Kumar, W. Bonin, A. Sundaresan, J. P. Attfield, C. N. R. Rao, A. Fuertes, *J. Mater. Chem. C* **2014**, *2*, 2212.
[10] J. Oró-Solé, L. Clark, W. Bonin, J. P. Attfield, A. Fuertes, *Chem. Commun.* **2013**, *49*, 2430.
[11] D. Logvinovich, J. Hejtmánek, K. Knížek, M. Maryško, N. Homazava, P. Tomeš, R. Aguiar, S. G. Ebbinghaus, A. Reller, A. Weidenkaff, *J. Appl. Phys.* **2009**, *105*, 023522.
[12] I. D. Fawcett, K. V. Ramanujachary, M. Greenblatt, *Mater. Res. Bull.* **1997**, *32*, 1565.
[13] J. Cabana, G. Rousse, A. Fuertes, M. R. Palacin, *J. Mater. Chem.* **2003**, *13*, 2402.
[14] J. Grins, P. O. Käll, G. Svensson, *J. Solid State Chem.* **1995**, *117*, 48.
[15] M. Retuerto, C. de La Calle, M. J. Martínez-Lope, F. Porcher, K. Krezhov, N. Menéndez, J. A. Alonso, *J. Solid State Chem.* **2012**, *185*, 18.
[16] a) Y. Inaguma, J.-M. Greneche, M.-P. Crosnier-Lopez, T. Katsumata, Y. Calage, J.-L. Fourquet, *Chem. Mater.* **2005**, *17*, 1386; b) Y. Tsujimoto, J. J. Li, K. Yamaura, Y. Matsushita, Y. Katsuya, M. Tanaka, Y. Shirako, M. Akaogi, E. Takayama-Muromachi, *Chem. Commun.* **2011**, *47*, 3263; c) Y. Tsujimoto, C. I. Sathish, Y.

Matsushita, K. Yamaura, T. Uchikoshi, *Chem. Commun.* **2014**, *50*, 5915; d) Y. Tsujimoto, K. Yamaura, T. Uchikoshi, *Inorg. Chem.* **2013**, *52*, 10211; e) T. Katsumata, M. Nakashima, Y. Inaguma, T. Tsurui, *Bull. Chem. Soc. Jpn.* **2012**, *85*, 397.
[17] C. Tassel, Y. Goto, Y. Kuno, J. Hester, M. Green, Y. Kobayashi, H. Kageyama, *Angew. Chem.* **2014**, *53*, 10377; *Angew. Chem. Int. Ed.* **2014**, *126*, 10545.
[18] M. Yang, J. A. Rodgers, L. C. Middler, J. Oró-Solé, A. B. Jorge, A. Fuertes, J. P. Attfield, *Inorg. Chem.* **2009**, *48*, 11498.
[19] E. Soignard, D. Machon, P. F. McMillan, J. Dong, B. Xu, K. Leinenweber, *Chem. Mater.* **2005**, *17*, 5465.
[20] a) Y. Inaguma, M. Yoshida, T. Katsumata, *J. Am. Chem. Soc.* **2008**, *130*, 6704; b) Y. Inaguma, A. Aimi, Y. Shirako, D. Sakurai, D. Mori, H. Kojitani, M. Akaogi, M. Nakayama, *J. Am. Chem. Soc.* **2014**, *136*, 2748; c) A. Aimi, T. Katsumata, D. Mori, D. Fu, M. Itoh, T. Kyômen, K. Hiraki, T. Takahashi, Y. Inaguma, *Inorg. Chem.* **2011**, *50*, 6392; d) T. Varga, A. Kumar, E. Vlahos, S. Denev, M. Park, S. Hong, T. Sanehira, Y. Wang, C. J. Fennie, S. K. Streiffer, X. Ke, P. Schiffer, V. Gopalan, J. F. Mitchell, *Phys. Rev. Lett.* **2009**, *103*, 047601.
[21] a) J. Ko, C. Prewitt, *Phys. Chem. Miner.* **1988**, *15*, 355; b) N. Ross, J. Ko, C. Prewitt, *Phys. Chem. Miner.* **1989**, *16*, 621.
[22] A. M. Arévalo-López, J. P. Attfield, *Phys. Rev. B* **2013**, *88*, 104416.
[23] a) S. J. Clarke, K. A. Hardstone, C. W. Michie, M. J. Rosseinsky, *Chem. Mater.* **2002**, *14*, 2664; b) E. Günther, R. Hagenmayer, M. Jansen, *Z. Anorg. Allg. Chem.* **2000**, *626*, 1519; c) M. Yang, J. Oró-Solé, J. A. Rodgers, A. B. Jorge, A. Fuertes, J. P. Attfield, *Nat. Chem.* **2011**, *3*, 47.
[24] I. D. Brown, R. D. Shannon, *Acta Crystallogr. Sect. A* **1973**, *29*, 266.
[25] J. Rodríguez-Carvajal, *Physica B* **1993**, *192*, 55.
[26] a) R. H. Mitchell, *Perovskites: Modern and Ancient*, Almaz Press, Ontario, **2002**; b) P. Woodward, *Acta Crystallogr. Sect. B* **1997**, *53*, 44.
[27] A. Glazer, *Acta Crystallogr. Sect. B* **1972**, *28*, 3384.
[28] a) A. Gukasov, U. Steigenberger, S. N. Barilo, S. A. Guretskii, *Physica B* **1997**, *234–236*, 760; b) J. Jeong, E. A. Goremychkin, T. Guidi, K. Nakajima, G. S. Jeon, S.-A. Kim, S. Furukawa, Y. B. Kim, S. Lee, V. Kiryukhin, S. W. Cheong, J.-G. Park, *Phys. Rev. Lett.* **2012**, *108*, 077202; c) G. Gorodetsky, *J. Phys. Chem. Solids* **1969**, *30*, 1745; d) S. M. Shapiro, J. D. Axe, J. P. Remeika, *Phys. Rev. B* **1974**, *10*, 2014.
[29] a) G. Matsumoto, *J. Phys. Soc. Jpn.* **1970**, *29*, 606; b) E. O. Wollan, W. C. Koehler, *Phys. Rev.* **1955**, *100*, 545.
[30] T. Takeda, Y. Yamaguchi, H. Watanabe, *J. Phys. Soc. Jpn.* **1972**, *33*, 967.
[31] T. Kimura, S. Ishihara, H. Shintani, T. Arima, K. T. Takahashi, K. Ishizaka, Y. Tokura, *Phys. Rev. B* **2003**, *68*, 060403.
[32] S. Quezel, F. Tcheou, J. Rossat-Mignod, G. Quezel, E. Roudaut, *Physica B + C* **1977**, *86–88*, *Part 2*, 916.
[33] A. A. Belik, N. Tsujii, H. Suzuki, E. Takayama-Muromachi, *Inorg. Chem.* **2007**, *46*, 8746.
[34] S. Lei, L. Liu, C. Wang, C. Wang, D. Guo, S. Zeng, B. Cheng, Y. Xiao, L. Zhou, *J. Mater. Chem. A* **2013**, *1*, 11982.
[35] C. J. Fennie, *Phys. Rev. Lett.* **2008**, *100*, 167203.
[36] Y. Inaguma, K. Tanaka, T. Tsuchiya, D. Mori, T. Katsumata, T. Ohba, K.-i. Hiraki, T. Takahashi, H. Saitoh, *J. Am. Chem. Soc.* **2011**, *133*, 16920.
[37] M. Markkula, A. M. Arevalo-Lopez, A. Kusmartseva, J. A. Rodgers, C. Ritter, H. Wu, J. P. Attfield, *Phys. Rev. B* **2011**, *84*, 094450.
[38] a) T. Kimura, *Annu. Rev. Mater. Res.* **2007**, *37*, 387; b) Y. Tokura, S. Seki, *Adv. Mater.* **2010**, *22*, 1554.
[39] K. Page, M. W. Stoltzfus, Y.-I. Kim, T. Proffen, P. M. Woodward, A. K. Cheetham, R. Seshadri, *Chem. Mater.* **2007**, *19*, 4037.
[40] T. Kimura, T. Goto, H. Shintani, K. Ishizaka, T. Arima, Y. Tokura, *Nature* **2003**, *426*, 55.
[41] G. Lawes, A. B. Harris, T. Kimura, N. Rogado, R. J. Cava, A. Aharony, O. Entin-Wohlman, T. Yildirim, M. Kenzelmann, C. Broholm, A. P. Ramirez, *Phys. Rev. Lett.* **2005**, *95*, 087205.
[42] A. H. Arkenbout, T. T. M. Palstra, T. Siegrist, T. Kimura, *Phys. Rev. B* **2006**, *74*, 184431.
[43] T. Kimura, J. C. Lashley, A. P. Ramirez, *Phys. Rev. B* **2006**, *73*, 220401.
[44] T. Kimura, Y. Sekio, H. Nakamura, T. Siegrist, A. P. Ramirez, *Nat. Mater.* **2008**, *7*, 291.
[45] G. Hitoki, T. Takata, J. N. Kondo, M. Hara, H. Kobayashi, K. Domen, *Chem. Commun.* **2002**, 1698.
[46] V. Petříček, M. Dušek, L. Palatinus, *Z. Kristallogr.* **2014**, *229*, 345.

